Enhancing Singlet Oxygen Generation in Conjugates of Silicon Nanocrystals and Organic Photosensitizers

Deski Beri[1], Marius Jakoby[1], Dmitry Busko[1], Bryce S. Richards[1,2]* and Andrey Turshatov[1]*

[1] Institute of Microstructure Technology, Karlsruhe Institute of Technology, Eggenstein-Leopoldshafen, Germany, [2] Light Technology Institute, Karlsruhe Institute of Technology, Karlsruhe, Germany

Silicon nanocrystals (SiNCs) are regarded as a green and environmentally friendly material when compared with other semiconductor nanocrystals. Ultra-small SiNCs (with the size 4.6–5.2 nm) demonstrate strong UV absorption and photoluminescence in the near infrared (NIR) range with the high photoluminescence quantum yield (PLQY) up to 60%. In contrast to nanoporous silicon, ultra-small SiNCs do not possess an intrinsic ability to generate singlet oxygen ($^1O_2$). However, we demonstrate that SiNC-dye conjugates synthesized *via* microwave assistant hydrosilylation reaction produce $^1O_2$ with moderate quantum yield (Φ_Δ) up to 27% in cyclohexane. These interesting results were obtained *via* measurements of singlet oxygen phosphorescence at 1,270 nm. SiNCs play an important role in the production of singlet oxygen as SiNCs harvest UV and blue radiation and transfer absorbed energy to a triplet state of the attached dyes. It increases the population of the triplet states and leads to the enhancement of the singlet oxygen generation. Simultaneously, the SiNC-dye conjugates demonstrate NIR luminescence with the PLQY up to 22%. Thus, the luminescence behavior and photosensitizing properties of the SiNC-dye conjugates can attract interest as a new multifunctional platform in the field of bio-applications.

Keywords: singlet oxygen, silicon nanocrystals, photosensitizers, NIR luminescence, microwave synthesis

INTRODUCTION

Singlet oxygen ($^1O_2$) is an extremely reactive species and powerful oxidant for many types of organic materials (Ogilby, 2010). The study of $^1O_2$ has attracted increasing attention due to its potential applications in many fields such as chemical synthesis (Manfrin et al., 2019), photocatalysis (Nosaka and Nosaka, 2017), water purification (García-Fresnadillo, 2018), and photodynamic therapy of cancer (Wang et al., 2004; Vlaskin et al., 2009; Ghogare and Greer, 2016). In chemistry, $^1O_2$ has been used to produced oxygenated hydrocarbons such as endoperoxide (Ahuja et al., 2018), deoxetanes (Camussi et al., 2019), as well as hydroperoxide and phosphine oxide for biomimetic organic synthesis of natural products and drugs (You and Nam, 2014). In the field of water treatment, $^1O_2$ has demonstrated its efficiency in the degradation of water born pollutants (Lyubimenko et al., 2019). In photodynamic therapy, $^1O_2$ has displayed a huge potential to destroy cancer cells (Campillo et al., 2019; Sun et al., in press). When a source of $^1O_2$ is selectively delivered to a tumor affected tissue, $^1O_2$ can react with many biological molecules—amino acid

residues in proteins and the nucleobases in DNA and RNA resulting in photo induced degradation of cancer cells (Castano et al., 2004; Yang et al., 2019).

The most important conventional method to produce $^1O_2$ is irradiation of photosensitizers (PSs) with ultraviolet or visible (UV/Vis) light. In the past, many potential organic and inorganic PSs have been proposed, for example, organic chromophores (Yogo et al., 2005), metal complexes (Monro et al., 2019), metal organic frameworks (Hu et al., 2018; Zheng et al., 2018), semiconductor quantum dots (QDs) (Bakalova et al., 2004; Rakovich et al., 2010), graphene QDs (Ge et al., 2014), perovskite nanocrystals (Gu et al., 2020) as well as metal nanoparticles (Chadwick et al., 2016) and metal nanowires (Smith et al., 2015). Among these, organic chromophores have been most intensively studied for $^1O_2$ generation as they exhibit strong UV/Vis absorption, fast and efficient intersystem crossing (ISC), and a long triplet lifetime (Callaghan and Senge, 2018). When exposed to UV/Vis light, organic PSs produce a large number of long-lived triplet states, which transfer energy to the ground (triplet) molecular oxygen state *via* triplet energy transfer (Wang et al., 2004; Maisch et al., 2007). Despite the forbidden nature of ISC in quantum mechanics under the El-Sayed rule, this process can be partially allowed in organic systems if the ISC involves a change of the orbital type (Marian, 2012) or in systems with strong spin-vibronic coupling (Penfold et al., 2018). Heavy elements anchored to a chromophore can also significantly enhance the rate of population of the triplet state *via* spin–orbit effect (Marian, 2012). Recently, the population of triplet state *via* a SOCT (spin–orbit charge transfer)-ISC have been proved to be efficient for generation of $^1O_2$ in different organic and water media (Filatov, 2020).

Interestingly, it has also been observed that the abundant and non-toxic chemical element of silicon (Si) can also produce $^1O_2$. A pioneering work by Kovalev et al. (2002) described generation of $^1O_2$ using silicon nanocrystals (SiNCs) distributed in a solid state porous Si layer. Several follow-up communications reported generation of $^1O_2$ in organic and aqueous media by relatively large (with size 50–150 nm) porous SiNCs (Osminkina et al., 2011; Xiao et al., 2011). Photosensitization of $^1O_2$ using ultra-small blue-emitting silicon nanocrystals (SiNCs) with size of 3 ± 1 nm and short photoluminescence (PL) decay lifetime of 1 ns was described by Llansola Portolés et al. (2010). Unlike SiNCs with blue PL resulting from surface defects, $^1O_2$ generation with SiNCs demonstrating quantum confinement effect and optical properties similar to semiconductor QDs has not yet been reported. These SiNCs typically demonstrate strong UV absorption and bright long-lived PL (∼100 μs PL decay time) in the red and near-infrared (NIR) spectral range. The long-lived NIR PL and low toxicity (Durnev et al., 2010; Cao et al., 2017; Mazzaro et al., 2017; Pramanik et al., 2018; Zhi et al., 2018) of SiNCs attract high attention of researchers in many application fields (Mazzaro et al., 2017).

The conjugation of organic dyes and SiNCs is a little explored topic relevant for many potential applications. It is known that an interaction between dyes and QDs can modified photophysical properties of the both (Lu et al., 2020). In particularly, the triplet exciton transfer between a dye and QD rises strong interest

in the luminescent energy harvesting by singlet fission (Gray et al., 2020) and triplet fusion (Xia et al., 2020). Beside of that, QDs can enhance ISC in organic dyes anchored to their surface (Ahmed et al., 2015; Jin et al., 2019), that can be used for efficient generation of and $^1O_2$ for PDT and photocatalytic applications.

Recently, we investigated conjugates of SiNCs and organic chromophores (Beri et al., 2020) in order to enhance visible absorption of SiNCs. To our surprise, we observed significant quenching SiNCs PL induced by organic chromophores covalently attached to the surface of SiNCs. We postulated that the quenching of the PL signal can originate from energy transfer from the SiNCs to the triplet state of the anchored dye molecule. These interesting findings motivated us to investigate in detail the role of SiNCs in photosensitization of the dye triplet state and a possible use of this process for generation of $^1O_2$.

In the current paper, we anchored two different perylene derivatives to the surface of SiNCs using a thermal hydrosilylation reaction. The perylene unit in the close proximity to the surface of SiNCs plays the role of an energy acceptor mediating the energy transfer from SiNCs to the triplet state of molecular oxygen. Utilizing this mechanism of the $^1O_2$ generation, we intended to enhance the potential value of SiNCs as a non-toxic and environmentally friendly material to sensitize reactive $^1O_2$ for applications in chemical synthesis and photodynamic therapy.

MATERIALS AND METHODS

Silicon monoxide (99.9%, 325 mesh) and phenalenone (*phe*) (also known as perinaphtenone, 97%) were purchased from Sigma-Aldrich. Hydrofluoric acid (48%) was purchased from Fisher Scientific. Ethanol (98%), methanol (HPLC grade), toluene (99%+) were purchased from Merck. 1-hexene (C6) (99%) was purchased from Acros. Cyclohexane (spectroscopic grade) was purchased from Alfa Aesar. 3-ethynylperylene (*dye-1*) was purchased from Lumiprobe GmbH, Germany and 3-ethenylperylene (*dye-2*) was purchased from Fluorochem. Ltd, U.K. All chemicals were used without further purification and the chemical structure the most important substances are presented in **Figure 1A**.

Synthetic Methods
Silicon nanocrystals were produced by a top-down method using the disproportionation reaction of silicon monoxide (SiO$_x$), x < 1. The reaction initialized by annealing of 3.0 g SiO$_x$ powder in a quartz boat at 900°C for 60 min under continuous H$_2$/Ar (5:95%) flow. During this annealing process, the nucleation of SiNCs seeds inside a silicon dioxide matrix occurs (Hessel et al., 2012). Details regarding the annealing procedure can be found in the literature (Beri et al., 2018). After annealing, the sample was transferred to an agate mortar and ground.

Synthesis of Hydrogen Terminated SiNCs (H-SiNCs)
1.0 g the ground powder was transferred to a PTFE flask, followed by the addition of 10 ml absolute ethanol and stirring for 5 min. Subsequently, 10 ml of HF 48% was added to the flask and the solution was stirred for the next 2.5 h. In 50 ml PTFE separatory

FIGURE 1 | (A) Molecular structures of (i) phenalenone (*phe*), (ii) 3-ethynylperylene (*dye-1*), (iii) 3-ethenylperylene (*dye-2*), (iv) hexyl-functionalized SiNCs (*C6-SiNCs*), (v) 3-ethynylperylene/hexyl-functionalized SiNCs (*C6-1-SiNCs*) and (vi) 3-ethenylperylene/hexyl-functionalized SiNCs (*C6-2-SiNCs*); **(B)** Schematic representation of the hydrosilylation reaction of hydrogen-terminated SiNCs with dye and 1-hexene.

funnel, 15 mL of toluene was added followed by the addition of the ethanol/HF mixture. The separation of *H-SiNCs* was performed by extracting the non-polar (toluene) part from the polar (ethanol/HF) media. The toluene solution transferred to the centrifuge tube to remove the large particles. The centrifugation was performed at 2,000 rpm for 2 min. The big particles were discarded and the toluene solution was transferred to the G30 microwave (MW) tube (Anton Paar) and Ar was purged through the dispersion in order to remove dissolved O$_2$. These *H-SiNCs* was ready for further reaction inside the MW reactor.

Synthesis of Hexyl Terminated SiNCs (C6-SiNCs)

Five milliliter of 1-hexene (C6) injected into G30 MW tube with the solution of *H-SiNCs* in toluene and purged for another 20 min. The tube with the solution was heated at 230°C for 120 min inside the MW reactor (Anton Paar GmbH). Unreacted C6 and toluene were removed with rotary evaporator and *C6-SiNCs* were re-dispersed in cyclohexane.

Synthesis of dye Terminated SiNCs (C6-1-SiNCs and C6-2-SiNCs)

A solution of *dye-1* in toluene (2 mg in 10 ml of toluene) was added to the solution of *H-SiNCs* in the G30 MW tube and the resulted solution was purged with Ar for 20 min. The tube with the solution was heated at 230°C for 120 min inside the MW reactor (Anton Paar GmbH). Five milliliter of *C6* was injected into the tube and again purged with Ar for another 20 min. The reaction in the MW reactor was repeated at 230°C for another 120 min. The schematic representative of the synthetic method is shown in **Figure 1B**. The product of the reaction with a dark orange color was transferred to the rotary evaporator flask and unreacted *C6* as well as toluene were removed. The obtained solid powder was rinsed with MeOH/EtOH (1:1) to remove unreacted dye. The precipitate was further redispersed in *cyclohexane* and stored in a glovebox and will be referred to as *C6-1-SiNCs*. The same procedure was applied for synthesis of *C6-2-SiNCs*.

Sample Characterization
Size and Size Distribution

Transmission electron microscope (TEM) investigations were carried out on a TITAN 60–300 microscope at accelerating voltage 300 kV (**Figure S1**). Dynamic Light Scattering (DLS) using Anton Paar Litesizer 500 was used for characterization of the particle size distribution.

Absorption and Photoluminescence Excitation (PLE) Spectra

Absorption spectra were taken by UV-Vis-NIR spectrophotometer (Perkin Elmer Lambda 950). with a 2 nm resolution. Photoluminescence excitation (PLE) spectra were measured with a spectrofluorometer (Varian Cary Eclipse). The PLE scan was conducted monitoring the 800 nm emission (close to maximum peak of SiNCs emission) and exploring the excitation range from 300 to 550 nm.

Photoluminescence (PL) and Photoluminescence Quantum Yield (PLQY) Measurements

PLQY, PL-lifetimes and PL-emission were determined by the methods, which have been earlier described (Beri et al., 2020).

Singlet Oxygen Quantum Yields (Φ_Δ)

Samples (2.5 ml) dispersed in cyclohexane were placed in a quartz cuvette (Starna) with path length 1 cm were irradiated with 405 nm diode lasers (75 mW, DL-7146-1012S, Roithner Laser Technique GmbH) or with a narrow-linewidth Ti:Sa laser (45 mW, SolsTiS, EMM-532, M-Squared Lasers) for the 317.5 nm excitations. The PL of $^1O_2$ was measured with irradiance calibrated NIR spectrometer (NIRQuest 512-1.7, Ocean Optics) operating in 900–1,700 nm range. Integration time of 100 s was used for collection of the $^1O_2$ phosphorescence spectra. The quantum yield of singlet $^1O_2$ generation (Φ_Δ) was calculated in agreement with Equation 1 using the *phe* as quantum yield as standard:

$$\Phi_\Delta^x = \Phi_\Delta^R \frac{\left[S_{em}^x\right]}{\left[S_{em}^R\right]} \frac{\left[I_{abs}^R\right]}{\left[I_{abs}^x\right]} \tag{1}$$

where Φ_Δ^x and Φ_Δ^R are singlet oxygen quantum yields of the sample and the reference, respectively. $\left[S_{em}^x\right]$ and $\left[S_{em}^R\right]$ are integrated area of $^1O_2$ PL generated by the sample and the reference, while $\left[I_{abs}^x\right]$ and $\left[I_{abs}^R\right]$ are the number of absorbed photons by the sample and the reference. In case of the excitation with monochromatic light, absorption (% of absorbed light $\left[A_\%^x\right]$ and $\left[A_\%^R\right]$ at the excitation wavelength) of the sample and the reference can be used instead of $\left[I_{abs}^x\right]$ and $\left[I_{abs}^R\right]$.

The reported value of Φ_Δ^R for *phe* in cyclohexane is 92 ± 10% (Schmidt et al., 1994). The concentrations of two sets of *phe*, *dye-1*, *dye-2*, *C6-1-SiNCs*, and *C6-2-SiNCs* solutions were adjusted to have roughly similar absorbance (*a*) at 405 and 317.5 nm.

Temperature-Dependent Photoluminescence Measurements

Dye molecules are dispersed in cyclohexane and placed in quartz cuvette with a path length of 2 mm and purged with argon gas for 30 min. Subsequently, the cuvette was clamped to the cryostat sample holder (Cryospares A7-103) and placed inside the sample chamber of the closed cycle cryostat (Oxford Instruments, Optistat Dry TLEX). After evacuating the sample chamber to ~10^{-5}hPa, the chamber was flooded with helium (purity >99.999mol%) to improve thermal coupling between the sample and the heat exchanger of the cryostat. PL emission spectra were measured at 20K for both *dye-1* and *dye-2* samples. For

the excitation, a mode-locked ytterbium laser (Light Conversion, Pharos) with a pulse width of 190 fs and a repetition rate of 20 kHz was used. The 1028 nm output of the laser was converted to 440 nm using an optical parametric amplifier (Light Conversion, Orpheus) and second harmonic generator (Light Conversion, Lyra). The steady state photoluminescence spectra were recorded by a fiber-coupled UV/VIS spectrometer (Avantes, AvaSpec-2048L).

RESULT AND DISCUSSION

The molecular structures of the reference PS—*phe*, perylene derivatives *dye-1* and *dye-2*, as well as hexyl functionalized SiNCs (*C6-SiNCs*), hexyl-dye functionalized SiNCs (*C6-1-SiNCs* and *C6-2-SiNCs*) are shown in **Figure 1A**.

The unsaturated bonds of *dye*-1 and *dye*-2 can react with the surface of *H-SiNCs* resulting in dye-functionalized SiNCs. The obtained dye-functionalized SiNCs exhibit enhanced absorption in the visible range and broad NIR emission with maximum of 860 nm and PLQYs of 15 ± 1% (for *C6-1-SiNCs*) and 22 ± 1% (for *C6-2-SiNCs*) as shown in **Table 1**. To improve the stability of SiNCs during and after the passivation reaction (**Figure 1B**), 1-hexene was employed as an additional surface ligand. A detailed investigation of the photophysical properties of *C6-SiNCs*, *C6- 1-SiNCs* and *C6-2-SiNCs* have been reported previously (Beri et al., 2020). In this previous publication, we found that the anchored dyes reduce both the PLQY of the NIR emission of SiNCs as well as the luminescence lifetime (at the NIR PL peak). As the NIR PL peak of SiNCs does not overlap with the absorption peak of the dyes (observed between 350 and 500 nm), we assumed that the NIR PL of SiNCs is quenched by the triplet state of the dyes *via* Dexter energy transfer. The resulting enhancement of the dye triplet population in the *C6-1-SiNCs* and *C6-2-SiNCs* can be probed *via* measurements of the yield of $^1O_2$ generated by the triplet states of the dye. Thus, the main goal of the present study is to compare Φ_Δ under the direct excitation of the attached dyes (with 405 nm laser) and SiNCs (with 317.5 nm laser), with the two chosen wavelengths enabling this selectivity.

There are two well-established methods to determine the Φ_Δ. The first method uses a particular trap compound such as 9,10-dimethylanthracene (DMA), 1,3-diphenylisobenzofuran (DPBF), singlet oxygen sensor green, etc. (You, 2018). For instance, the DMA trap reacts specifically with $^1O_2$ to form peroxide. This chemical reaction results in changes of the absorption spectrum of DMA decaying with irradiation time. By measuring the absorption decay, the Φ_Δ could be determined quantitatively *via* the comparison with the absorption decay induced by a reference PS with a known Φ_Δ^R. The second method is based on measurements of $^1O_2$ phosphorescence and Equation 1. The radiative relaxation process from excited $^1O_2$ to the ground triplet state ($^1\Delta_g \rightarrow \, ^3\Sigma_g$) yields an emission at 1,270 nm with relatively long lifetime (ms-to-s, depending on solvent) (Khan and Kasha, 1979; DeRosa and Crutchley, 2002). Similar to the first method, it also requires a reference material with known Φ_Δ^R for the comparison of intensities of $^1O_2$ phosphorescence.

TABLE 1 | Absorbance (α), normalized intensity of $^1O_2$ phosphorescence (I_{em}), photoluminescence quantum yield (PLQY), and singlet oxygen quantum yields (Φ_Δ) measured with 317.5 nm and 405 nm lasers.

PS	a(317.5nm)	I_{em}[†]	a(405nm)	I_{em}[‡]	PLQY,%	Φ_Δ,%[†]	Φ_Δ,%[‡]
phe	0.576	1	0.760	1	–	92 ± 10*	92 ± 10*
dye-1	0.138	0.111	0.763	0.381	68 ± 1[‡,§]	45 ± 14	35 ± 5
dye-2	0.081	0.090	0.760	0.382	52 ± 1[‡,§]	56 ± 25	34 ± 5
C6-SiNc	0.780	–	0.773	–	33 ± 1[†,♦]	–	–
C6-1-SiNCs	0.576	0.213	0.693	0.264	15 ± 1[†,♦]	20 ± 5	27 ± 5
C6-2-SiNCs	0.331	0.052	n/a	n/a	22 ± 1[†,♦]	9 ± 6	n/a

[†] Corresponds to the 317.5 nm excitation; [‡] corresponds to the 405 nm excitation; *reference $\Phi_\Delta = 0.92 \pm 10$ (Schmidt et al., 1994) [§]PLQY of dyes visible emission integrated in the range 350–500 nm; [♦] PLQY of SiNCs NIR emission integrated in the range 650–1,000 nm; I_{em} was normalized using the emission of $^1O_2$ excited via phe ($I_{em} = 1$ for phe); The uncertainty of Φ_Δ was calculated in agreement with Equation S1 (**Supporting Information**). The uncertainty of PLQY measurements were earlier reported in Saleta Reig et al. (2020). The Φ_Δ for dye-2 under 405 excitation is not reported because luminescence of $^1O_2$ was too weak.

It should be noted that the first method has a significant disadvantage for the estimation of Φ_Δ. Several factors must be taken into account to determine the correct value of Φ_Δ, including: overlap of absorption spectra of the sample and trap; self-degradation of the trap; as well as trap decomposition induced by other reactive oxygen species. For instance, we were not able to measure Φ_Δ via either DMA or DPBF due to the spectral overlap with the broad absorption spectra of C6-1-SiNCs and C6-2-SiNCs. A subsequent attempt to use rubrene (absorbing in range 450–550 nm) as the $^1O_2$ trap also failed, as rubrene displayed a fast rate of the self-degradation upon irradiation with 405 nm and 317.5 nm lasers (**Figure S2**). Thus, the second method of the estimation of Φ_Δ based on the detection of $^1O_2$ phosphorescence was chosen as the most reliable.

Singlet Oxygen Generation With Dye-1 and Dye-2

Before conducting the experiments related to $^1O_2$ generation, the photostability of the reference PS—phe was evaluated (**Figure S3**). The degradation of 20% phe was found after long-time (1 h) irradiation of a solution of the reference PS in cyclohexane using 15 mW UV LED. Taking into account that acquisition of $^1O_2$ luminescence (using 317.5 nm laser with intensity of 45 mW) takes ~100 s, we considered the reference PS as photostable. When we were satisfied that the phe was photostable, we investigated $^1O_2$ generation by dye-1 and dye-2. Perylene by itself exhibits a very high PLQY of 94% in cyclohexane (Taniguchi et al., 2018) and is thus a very poor PS. However, perylene derivatives have demonstrated ability to generate $^1O_2$ with high quantum yield (Wu et al., 2010; Filatov et al., 2018; Blacha-Grzechnik et al., 2020). **Figures 2B,D** demonstrates phosphorescence of $^1O_2$ generated via photoexcitation of dye-1 and dye-2 solutions in cyclohexane via both 405 and 317.5 nm laser excitation. The concentration of solutions with dye-1, dye-2, and phe was adjusted to have similar absorption at the excitation wavelengths (**Figures 2A,C**). The absorption of the samples $A_\%^x$ was estimated from absorbance a_x using Equation 2:

$$A_\%^x = 100\% - 10^{(2 - a_x)}, \qquad (2)$$

where $A_\%^x$ is % of absorbed light and a_x is absorbance measured experimentally.

A calculation using Equation 1 gives the value of $\Phi_\Delta = 35 \pm 5\%$ for dye-1 and $\Phi_\Delta = 34 \pm 5\%$ for dye-2 when excited with the 405 nm laser. Measurements with the other excitation wavelength (317.5 nm) result to very weak $^1O_2$ phosphorescence with very high uncertainty in $\Phi_\Delta = 45 \pm 14\%$ (for dye-1) and $\Phi_\Delta = 56 \pm 25\%$ (for dye-2) because of the weak dye absorption at 317.5 nm.

Interestingly, the dyes demonstrate unusually large values of Φ_Δ together with large values of absolute PLQY of 68 ± 1% and 52 ± 1% measured for dye-1 and dye-2, respectively. Note, that absolute PLQYs were estimated in the integrating sphere and have a higher precision than Φ_Δ. To gain inside $^1O_2$ photosensitization we measured PLQY for dye solutions prepared inside a glovebox under oxygen-free conditions. We found PLQY of 98% for dye-1 and 80% for dye-2. The obtained result indicates that photosensitization of $^1O_2$ occurs solely via the excite singlet state in case of dye-1 and predominantly in case of dye-2. It appears that, around two-thirds of the excited singlet states relax via the radiative transition for dye-1, whereas around one-third of the excited singlets transfer the energy to oxygen molecules. For dye-2, ~50% of the excitation energy decaying via radiative relaxation, whereas the remainder (~30%) transfers the energy to oxygen. Earlier, the highest Φ_Δ of 67% for perylene-like molecules was reported for rather complex di-(perylenebisimide) derivatives (Wu et al., 2010). However, our measurements indicate that moderate Φ_Δ of 35 ± 5% can be achieved with the simple molecules, which can be produced without expensive and time-consuming multistep synthesis.

To obtain additional information about triplet states of dye-1 and dye-2, we measured the emission spectra of their glassy solutions (in cyclohexane) at low temperature (20 K). Assuming small, but non-zero probability of ISC, we expected to detect phosphorescence of dye-1 and dye-2 at low temperature. **Figure 3** demonstrates a comparison of PL spectra collected at room temperature and 20 K. Indeed, new emission bands appear in the low temperature spectra with maxima at 674 and 735 nm for dye-1 and 670 and 735 nm for dye-2. We attributed the appearance of these bands to the radiative T_1–S_0 transition. The position of these peaks is slightly blue-shifted

FIGURE 2 | (A) UV-Vis absorption spectra of solutions of *phe*, *dye-1*, and *dye-2* in cyclohexane used for the generation of $^1O_2$ with 405 nm laser; **(B)** $^1O_2$ phosphorescence excited *via* irradiation of solutions of *phe* and *dye-1* with 405 nm laser (75 mW); **(C)** UV-Vis absorption spectra of solutions of *phe*, *dye-1*, and *dye-2* in cyclohexane used for the generation of $^1O_2$ with 317.5 nm laser; **(D)** $^1O_2$ phosphorescence excited via irradiation of solutions of *phe*, *dye-1*, and *dye-2* with 317.5 nm laser (excitation intensity of 15 mW).

FIGURE 3 | Photoluminescence of **(A)** *dye-1* and **(B)** *dye-2* at temperature of 300 and 20 K. Dashed lines represent results of deconvolution of low-temperature photoluminescence using Gaussian peaks centered at 673 and 735 nm for *dye 1* and 610, 670, and 735 nm for *dye 2*.

FIGURE 4 | (A) UV-Vis absorption spectra of solutions of *phe, C6-SiNCs* and *C6-1-SiNCs* in cyclohexane used for the generation of $^1O_2$ with 405 nm laser; **(B)** $^1O_2$ phosphorescence excited *via* irradiation of solutions of *phe, C6-SiNCs* and *C6-1-SiNCs* with 405 nm laser (excitation intensity of 75 mW); **(C)** UV-Vis absorption spectra of solutions of *phe, C6-SiNCs, C6-1-SiNCs* and *C6-2-SiNCs* in cyclohexane used for the generation of $^1O_2$ with 317.5 nm laser; **(D)** $^1O_2$ phosphorescence excited via irradiation of solutions of *phe, C6-SiNCs, C6-1-SiNCs* and *C6-2-SiNCs* with 317.5 nm laser (excitation intensity of 45 mW).

when compared with the position of T_1 state of 800–850 nm in the unsubstituted perylene molecule (Turshatov et al., 2012). However, it is highly likely that the dye triplet with the T_1 energy of ~1.7 eV (740 nm) can be excited *via* the energy transfer process utilizing the energy of SiNCs with PL in range 1.2–1.9 eV (650–1,000 nm).

Singlet Oxygen Generation With C6-1-SiNCs and C6-2-SiNCs

The chemical reaction of the dyes with *H-SiNCs* yields a product of conjugation that demonstrates absorption of both components. The PLE spectra of *C6-1-SiNCs* (**Figure S4**) and *C6-2-SiNCs* (**Figure S5**) confirm the dye attachment. The excitation of SiNCs becomes possible *via* dye excitation in the range of 400–450 nm, which indicates the very short distance between dyes and SiNCs. In contrast, the physical mixture of *C6-SiNCs* and the dyes does not demonstrate NIR luminescence when the sample is excited with blue light (400–450 nm).

It should be pointed out that the irradiation of *C6-1-SiNCs* and *C6-2-SiNCs* with 317.5 and 405 nm lasers excites different species.

The 405 nm laser mainly excites the dye molecule anchored to the surface of SiNCs, whereas the 317.5 nm laser directly excites SiNCs as the dyes exhibit an absorption minimum at this wavelength. The results of the calculation with Equation 1 (using the data presented in **Figures 4A,B** and **Table 1**) indicate that *C6-1-SiNCs* excited with 405 nm laser generate $^1O_2$ with $\Phi_\Delta = 27 \pm 5\%$. This quantum yield is lower than Φ_Δ of pure *dye-1*. However, the experiment emphasizes that the *C6-1-SiNCs* conjugate exhibits synergistic behavior. Under blue light excitation at room temperature, the nanoparticles demonstrate NIR emission (originating from the SiNCs core) with PLQY of $15 \pm 1\%$ and $^1O_2$ generation (originated from the anchored dye). Thus, this new conjugate can attract potential interest in photomedicine as a new chemical agent combining properties of PS and a NIR phosphor.

The irradiation of *C6-1-SiNCs* with the 317.5 nm laser should lead to selective excitation of SiNCs. To the best of our knowledge, the SiNCs synthesized from SiO_x are not able to generate $^1O_2$. Indeed, the excitation of *C6-SiNCs* with 317.5 and 405 nm lasers do not produce $^1O_2$ phosphorescence (**Figures 4B,D**). However, the excitation of the *C6-1-SiNCs*
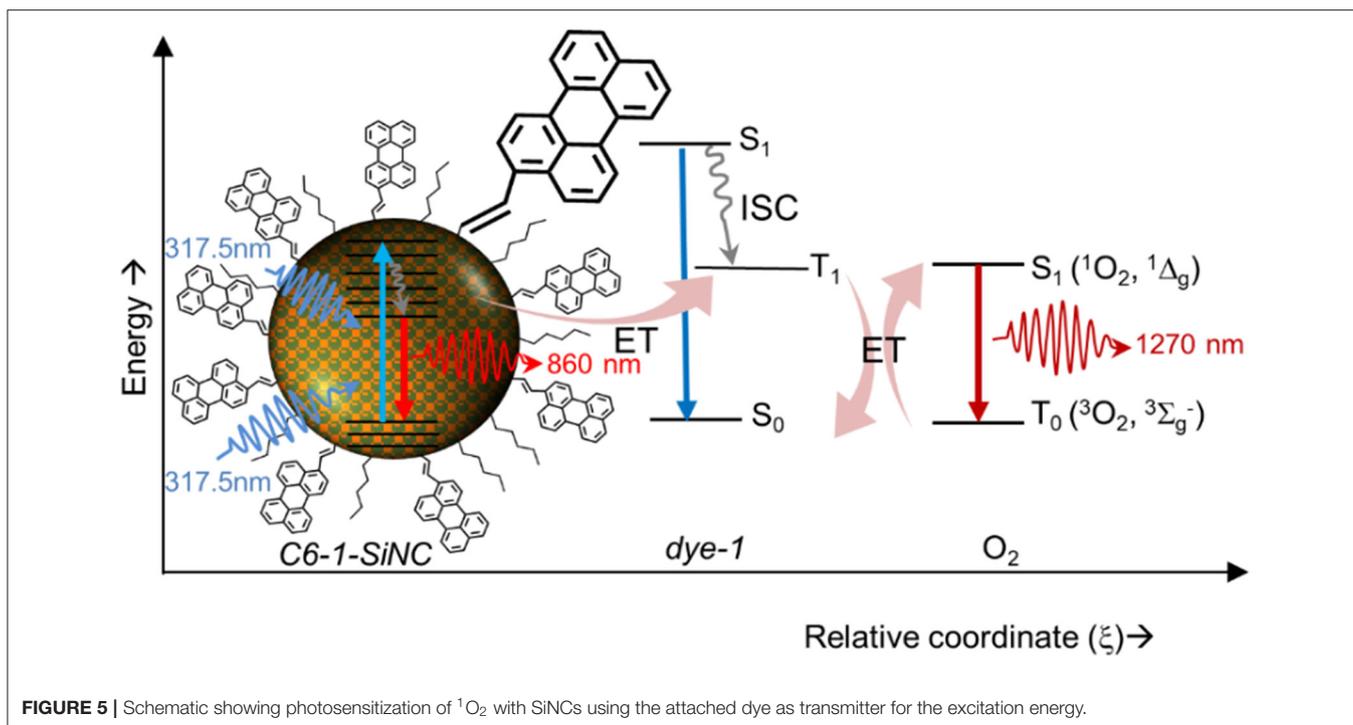
FIGURE 5 | Schematic showing photosensitization of $^1O_2$ with SiNCs using the attached dye as transmitter for the excitation energy.

conjugate with the 317.5 nm laser results in $^1O_2$ phosphorescence with $\Phi_\Delta = 20 \pm 5\%$. The enhancement factor (F) of $^1O_2$ oxygen generation with UV light (317.5 nm) for *C6-1-SiNCs* vs. *dye-1* can be determined using Equation 3:

$$F = \frac{[\Phi_\Delta^{(C6)-1-SiNCs}]}{[\Phi_\Delta^{dye}]} \frac{[a_{(C6)-1-SiNCs}]}{[a_{dye}]} \qquad (3)$$

where we assume that two solutions (*C6-1-SiNCs* and *dye-1*) exhibit similar absorbance at the 450 nm peak (indication of similar perylene concentration); $\Phi_\Delta^{(C6)-1-SiNCs}$ and Φ_Δ^{dye} are quantum yields of $^1O_2$ generation measured at the 317.5 nm excitation for the *C6-1-SiNCs* conjugate and *dye-1,* respectively; $a_{(C6)-1-SiNCs}$ and a_{dye} are absorbance of the two solutions at 317.5 nm.

The enhancement factor $F = 2.3$ indicates that the solution with *C6-1-SiNCs* is able produce 2.3 times more $^1O_2$ then the solution with *dye-1* with similar concentration of perylene chromophore. We performed here the calculation of F only for one single wavelength (317.5 nm). However, this conclusion can be also valid for the broad UV range ($\sim$300–350 nm) with strong absorption of SiNCs. Thus, the *C6-1-SiNCs* conjugate demonstrate the ability of efficient $^1O_2$ generation over very broad spectral range utilizing the absorption of SiNCs ($\sim$300–350 nm) and the absorption of dye-1 ($\sim$350–460 nm).

It has been mentioned in our previous publication (Beri et al., 2020) that energy transfer from SiNCs to the triplet state of *dye-2* is less efficient. This observation was also confirmed in the experiment with $^1O_2$ generation. The *C6-2-SiNCs* conjugate

exhibits significant lower $\Phi_\Delta = 9 \pm 6\%$ under excitation with UV light (317.5 nm) (**Figures 4C,D** and **Table 1**).

Energy Transfer From SiNCs to Perylene Chromophore

The schematic at **Figure 5** displays a $^1O_2$ generation pathway under UV excitation of *C6-1-SiNCs.* Under excitation with 317.5 nm laser, the crystals emit NIR photons with the wavelength of 860 nm. At the same time, the excitation energy can be transferred to the triplet state of the dye. The triplet state interacts with molecular oxygen. The interaction produces $^1O_2$ that emits NIR photons with the wavelength of 1,270 nm with the overall quantum efficiency of $^1O_2$ production around 20%

Finally, we were able to evaluate the efficiency of energy transfer (η_{ET}) from the SiNC core to the perylene chromophore from the calculations of Φ_Δ. At 317.5 nm excitation, the efficiency of the energy transfer can be calculated using Equation 4 and the values contained in **Table 1**:

$$\eta_{ET} = \frac{[\Phi_\Delta^{317.5nm}] - [P_{dye}^{317.5nm}][\Phi_\Delta^{405nm}]}{[P_{SiNCs}^{317.5nm}][\Phi_\Delta^{405nm}]}, \qquad (4)$$

where η_{ET} is energy transfer efficiency from SiNCs to attached dyes, $[\Phi_\Delta^{317.5nm}] = 20\%$ is the quantum yield of $^1O_2$ generation by *C6-1-SiNCs* under 317.5 nm excitation; $[\Phi_\Delta^{405nm}] = 27\%$ is the quantum yield of $^1O_2$ generation by *C6-1-SiNCs* under 405 nm excitation; $[P_{dye}^{317.5nm}] = 24\%$ is a part of the excitation light (with wavelength of 317.5 nm) absorbed by the dye; $[P_{SiNCs}^{317.5nm}] = 76\%$ is a part of the excitation light (with wavelength of 317.5 nm) absorbed by the SiNC core.

The calculation of η_{ET} with Equation 4 gives a value of 66%. This value is in very good agreement with the value of η_{ET} of 55% calculated using PL lifetimes of the NIR emission of *C6-SiNCs* and *C6-1-SiNCs* nanocrystals (Beri et al., 2020).

CONCLUSIONS

The SiNCs were modified with organic dyes *via* the hydrosilylation reaction in the microwave reactor. The SiNC-dye conjugates were investigated for the first time within the context of singlet oxygen generation. The singlet oxygen yield was determined *via* measurements of singlet oxygen phosphorescence (at 1,270 nm) in cyclohexane solutions using the comparison with the singlet oxygen phosphorescence produced by the reference PS—*phe*. The Φ_Δ values were estimated for two excitation wavelengths: 317.5 nm at 405 nm. The calculation of Φ_Δ for the *C6- 1- SiNC* conjugate results $\Phi_\Delta = 27 \pm 5\%$ and $\Phi_\Delta = 20 \pm 5\%$ for 405 nm and 317.5 nm excitations, respectively. We attributed high yield of singlet oxygen generation under 317.5 nm with efficient energy transfer from photoexcited SiNCs to the triplet states of attached molecules of *dye-1*. In contrast to *dye-1*, *dye-2* is a less efficient acceptor for SiNCs. As results, the Φ_Δ value of the *C6-2-SiNCs* conjugates is smaller—$\Phi_\Delta = 9 \pm 6\%$. We assumed that *C6-1-SiNCs* demonstrate high Φ_Δ over entire absorption spectrum of *C6-1-SiNCs* ($\sim$300–460 nm). Thus, this finding indicates a large potential of the dye modified SiNCs for the production of singlet oxygen.

DATA AVAILABILITY STATEMENT

All datasets generated for this study are included in the article/**Supplementary Material**.

AUTHOR CONTRIBUTIONS

DBe: synthesis of the dye functionalized SiNCs, characterization of SiNCs, measurement of singlet oxygen, evaluation and interpretation of the data, and writing. MJ: temperature dependent photoluminescence measurement. DBu: measurement of singlet oxygen. BR: supervision, data interpretation, and writing. AT: development of a paper concept, supervision data interpretation, and writing. All authors contributed to the manuscript revision, read, and approved the submitted version.

FUNDING

ACKNOWLEDGMENTS

SUPPLEMENTARY MATERIAL

The Supplementary Material for this article can be found online at: https://www.frontiersin.org/articles/10.3389/fchem.2020.00567/full#supplementary-material

REFERENCES

Ahmed, G. H., Aly, S. M., Usman, A., Eita, M. S., Melnikov, V. A., and Mohammed, O. F. (2015). Quantum confinement-tunable intersystem crossing and the triplet state lifetime of cationic porphyrin–CdTe quantum dot nano-assemblies. *Chem. Commun.* 51, 8010–8013. doi: 10.1039/C5CC01542A

Ahuja, S., Raghunathan, R., Kumarasamy, E., Jockusch, S., and Sivaguru, J. (2018). Realizing the photoene reaction with alkenes under visible light irradiation and bypassing the favored [2+2]-photocycloaddition. *J. Am. Chem. Soc.* 140, 13185–13189. doi: 10.1021/jacs.8b08100

Bakalova, R., Ohba, H., Zhelev, Z., Ishikawa, M., and Baba, Y. (2004). Quantum dots as photosensitizers? *Nat. Biotechnol.* 22, 1360–1361. doi: 10.1038/nbt1104-1360

Beri, D., Busko, D., Mazilkin, A., Howard, I. A., Richards, B. S., and Turshatov, A. (2018). Highly photoluminescent and stable silicon nanocrystals functionalized via microwave-assisted hydrosilylation. *RSC Adv.* 8, 9979–9984. doi: 10.1039/C7RA13577G

Beri, D., Jakoby, M., Howard, I. A., Busko, D., Richards, B. S., and Turshatov, A. (2020). Improved photon absorption in dye-functionalized silicon nanocrystals synthesized via microwave-assisted hydrosilylation. *Dalton Trans.* 49, 2290–2299. doi: 10.1039/C9DT04497C

Blacha-Grzechnik, A., Drewniak, A., Walczak, K. Z., Szindler, M., and Ledwon, P. (2020). Efficient generation of singlet oxygen by perylene diimide photosensitizers covalently bound to conjugate polymers. *J. Photochem. Photobiol. A* 388:112161. doi: 10.1016/j.jphotochem.2019.112161

Callaghan, S., and Senge, M. O. (2018). The good, the bad, and the ugly – controlling singlet oxygen through design of photosensitizers and delivery systems for photodynamic therapy. *Photochem. Photobiol. Sci.* 17, 1490–1514. doi: 10.1039/C8PP00008E

Campillo, N., Falcones, B., Otero, J., Colina, R., Gozal, D., Navajas, D., et al. (2019). Differential oxygenation in tumor microenvironment modulates macrophage and cancer cell crosstalk: novel experimental setting and proof of concept. *Front. Oncol.* 9:43. doi: 10.3389/fonc.2019.00043

Camussi, I., Mannucci, B., Speltini, A., Profumo, A., Milanese, C., Malavasi, L., et al. (2019). g-C3N4 - singlet oxygen made easy for organic synthesis: scope and limitations. *Acs Sustain. Chem. Eng.* 7, 8176–8182. doi: 10.1021/acssuschemeng.8b06164

Cao, Z., Peng, F., Hu, Z., Chu, B., Zhong, Y., Su, Y., et al. (2017). *In vitro* cellular behaviors and toxicity assays of small-sized fluorescent silicon nanoparticles. *Nanoscale* 9, 7602–7611. doi: 10.1039/C7NR00530J

Castano, A. P., Demidova, T. N., and Hamblin, M. R. (2004). Mechanisms in photodynamic therapy: part one—photosensitizers, photochemistry and cellular localization. *Photodiagn. Photodyn. Ther.* 1, 279–293. doi: 10.1016/S1572-1000(05)00007-4

Chadwick, S. J., Salah, D., Livesey, P. M., Brust, M., and Volk, M. (2016). Singlet oxygen generation by laser irradiation of gold nanoparticles. *J. Phys. Chem. C* 120, 10647–10657. doi: 10.1021/acs.jpcc.6b02005

DeRosa, M. C., and Crutchley, R. J. (2002). Photosensitized singlet oxygen and its applications. *Coord. Chem. Rev.* 233–234, 351–371. doi: 10.1016/S0010-8545(02)00034-6

Durnev, A. D., Solomina, A. S., Daugel-Dauge, N. O., Zhanataev, A. K., Shreder, E. D., Nemova, E. P., et al. (2010). Evaluation of genotoxicity and reproductive toxicity of silicon nanocrystals. *Bull. Exp. Biol. Med.* 149, 445–449. doi: 10.1007/s10517-010-0967-3

Filatov, M. A. (2020). Heavy-atom-free BODIPY photosensitizers with intersystem crossing mediated by intramolecular photoinduced electron transfer. *Org. Biomol. Chem.* 18, 10–27. doi: 10.1039/C9OB02170A

Filatov, M. A., Karuthedath, S., Polestshuk, P. M., Callaghan, S., Flanagan, K. J., Wiesner, T., et al. (2018). BODIPY-pyrene and perylene dyads as heavy-atom-free singlet oxygen sensitizers. *Chemphotochem* 2, 606–615. doi: 10.1002/cptc.201800020

García-Fresnadillo, D. (2018). Singlet oxygen photosensitizing materials for point-of-use water disinfection with solar reactors. *Chemphotochem* 2, 512–534. doi: 10.1002/cptc.201800062

Ge, J., Lan, M., Zhou, B., Liu, W., Guo, L., Wang, H., et al. (2014). A graphene quantum dot photodynamic therapy agent with high singlet oxygen generation. *Nat. Commun.* 5:4596. doi: 10.1038/ncomms5596

Ghogare, A. A., and Greer, A. (2016). Using singlet oxygen to synthesize natural products and drugs. *Chem. Rev.* 116, 9994–10034. doi: 10.1021/acs.chemrev.5b00726

Gray, V., Allardice, J. R., Zhang, Z., Dowland, S., Xiao, J., Petty, A. J., et al. (2020). Direct vs delayed triplet energy transfer from organic semiconductors to quantum dots and implications for luminescent harvesting of triplet excitons. *ACS Nano* 14, 4224–4234. doi: 10.1021/acsnano.9b09339

Gu, K., Wang, Y., Shen, J., Zhu, J., Zhu, Y., and Li, C. (2020). Effective singlet oxygen generation in silica-coated CsPbBr3 quantum dots through energy transfer for photocatalysis. *Chemsuschem* 13, 682–687. doi: 10.1002/cssc.201903157

Hessel, C. M., Reid, D., Panthani, M. G., Rasch, M. R., Goodfellow, B. W., Wei, J. W., et al. (2012). Synthesis of ligand-stabilized silicon nanocrystals with size-dependent photoluminescence spanning visible to near-infrared wavelengths. *Chem. Mater.* 24, 393–401. doi: 10.1021/cm2032866

Hu, F., Mao, D., Kenry, W.ang, Y., Wu, W., Zhao, D., Kong, D., et al. (2018). Metal–organic framework as a simple and general inert nanocarrier for photosensitizers to implement activatable photodynamic therapy. *Adv. Funct. Mater.* 28:1707519. doi: 10.1002/adfm.201707519

Jin, T., Uhlikova, N., Xu, Z., Zhu, Y., Huang, Y., Egap, E., et al. (2019). Enhanced triplet state generation through radical pair intermediates in BODIPY-quantum dot complexes. *J. Chem. Phys.* 151:241101. doi: 10.1063/1.5136045

Khan, A. U., and Kasha, M. (1979). Direct spectroscopic observation of singlet oxygen emission at 1268 nm excited by sensitizing dyes of biological interest in liquid solution. *Proc. Natl. Acad. Sci. U.S.A.* 76, 6047–6049. doi: 10.1073/pnas.76.12.6047

Kovalev, D., Gross, E., Kunzner, N., Koch, F., Timoshenko, V. Y., and Fujii, M. (2002). Resonant electronic energy transfer from excitons confined in silicon nanocrystals to oxygen molecules. *Phys. Rev. Lett.* 89, 137401. doi: 10.1103/PhysRevLett.89.137401

Llansola Portolés, M. J., David Gara, P. M., Kotler, M. L., Bertolotti, S., San Román, E., Rodríguez, H. B., et al. (2010). Silicon nanoparticle photophysics and singlet oxygen generation. *Langmuir* 26, 10953–10960. doi: 10.1021/la100980x

Lu, H., Huang, Z., Martinez, M. S., Johnson, J. C., Luther, J. M., and Beard, M. C. (2020). Transforming energy using quantum dots. *Energy Environ. Sci.* 13, 1347–1376. doi: 10.1039/C9EE03930A

Lyubimenko, R., Busko, D., Richards, B. S., Schäfer, A. I., and Turshatov, A. (2019). Efficient photocatalytic removal of methylene blue using a metalloporphyrin–poly(vinylidene fluoride) hybrid membrane in a flow-through reactor. *ACS Appl. Mater. Interfaces* 11, 31763–31776. doi: 10.1021/acsami.9b04601

Maisch, T., Baier, J., Franz, B., Szeimies, R., Landthaler, M., and Baumler, W. (2007). The role of singlet oxygen and oxygen concentration in photodynamic inactivation of bacteria. *Proc. Natl. Acad. Sci. U.S.A.* 104, 7223–7228. doi: 10.1073/pnas.0611328104

Manfrin, A., Borduas-Dedekind, N., Lau, K., and Mcneill, K. (2019). Singlet oxygen photooxidation of peptidic oxazoles and thiazoles. *J. Org. Chem.* 84, 2439–2447. doi: 10.1021/acs.joc.8b02684

Marian, C. M. (2012). Spin–orbit coupling and intersystem crossing in molecules. *WIREs Comput. Mol. Sci.* 2, 187–203. doi: 10.1002/wcms.83

Mazzaro, R., Romano, F., and Ceroni, P. (2017). Long-lived luminescence of silicon nanocrystals: from principles to applications. *Phys. Chem. Chem. Phys.* 19, 26507–26526. doi: 10.1039/C7CP05208A

Monro, S., Colón, K. L., Yin, H., Roque, J., Konda, P., Gujar, S., et al. (2019). Transition metal complexes and photodynamic therapy from a tumor-centered approach: challenges, opportunities, and highlights from the development of TLD1433. *Chem. Rev.* 119, 797–828. doi: 10.1021/acs.chemrev.8b00211

Nosaka, Y., and Nosaka, A. Y. (2017). Generation and detection of reactive oxygen species in photocatalysis. *Chem. Rev.* 117, 11302–11336. doi: 10.1021/acs.chemrev.7b00161

Ogilby, P. R. (2010). Singlet oxygen: there is indeed something new under the sun. *Chem. Soc. Rev.* 39, 3181–3209. doi: 10.1039/b926014p

Osminkina, L. A., Gongalsky, M. B., Motuzuk, A. V., Timoshenko, V. Y., and Kudryavtsev, A. A. (2011). Silicon nanocrystals as photo- and sono-sensitizers for biomedical applications. *Appl. Phys. B* 105, 665–668. doi: 10.1007/s00340-011-4562-8

Penfold, T. J., Gindensperger, E., Daniel, C., and Marian, C. M. (2018). Spin-vibronic mechanism for intersystem crossing. *Chem. Rev.* 118, 6975–7025. doi: 10.1021/acs.chemrev.7b00617

Pramanik, S., Hill, S. K. E., Zhi, B., Hudson-Smith, N. V., Wu, J. J., White, J. N., et al. (2018). Comparative toxicity assessment of novel Si quantum dots and their traditional Cd-based counterparts using bacteria models *Shewanella oneidensis* and *Bacillus subtilis*. *Environ. Sci. Nano* 5, 1890–1901. doi: 10.1039/C8EN00332G

Rakovich, A., Savateeva, D., Rakovich, T., Donegan, J. F., Rakovich, Y. P., Kelly, V., et al. (2010). CdTe quantum dot/dye hybrid system as photosensitizer for photodynamic therapy. *Nanoscale Res. Lett.* 5, 753–760. doi: 10.1007/s11671-010-9553-x

Saleta Reig, D., Grauel, B., Konyushkin, V. A., Nakladov, A. N., Fedorov, P. P., Busko, D., et al. (2020). Upconversion properties of SrF2:Yb3+,Er3+ single crystals. *J. Mater. Chem. C.* 8, 4093–4101. doi: 10.1039/C9TC06591A

Schmidt, R., Tanielian, C., Dunsbach, R., and Wolff, C. (1994). Phenalenone, a universal reference compound for the determination of quantum yields of singlet oxygen O2(1-Delta-G) sensitization. *J. Photochem. Photobiol. A* 79, 11–17. doi: 10.1016/1010-6030(93)03746-4

Smith, J. G., Faucheaux, J. A., and Jain, P. K. (2015). Plasmon resonances for solar energy harvesting: a mechanistic outlook. *Nano Today* 10, 67–80. doi: 10.1016/j.nantod.2014.12.004

Sun, Y., Zhao, D., Wang, G., Wang, Y., Cao, L., Sun, J., et al. (in press). Recent progress of hypoxia-modulated multifunctional nanomedicines to enhance photodynamic therapy: opportunities, challenges, and future development. *Acta Pharm. Sin. B.* doi: 10.1016/j.apsb.2020.01.004

Taniguchi, M., Du, H., and Lindsey, J. S. (2018). PhotochemCAD 3: diverse modules for photophysical calculations with multiple spectral databases. *Photochem. Photobiol.* 94, 277–289. doi: 10.1111/php.12862

Turshatov, A., Busko, D., Avlasevich, Y., Miteva, T., Landfester, K., and Baluschev, S. (2012). Synergetic effect in triplet–triplet annihilation upconversion: highly efficient multi-chromophore emitter. *Chemphyschem* 13, 3112–3115. doi: 10.1002/cphc.201200306

Vlaskin, V. A., Beaulac, R., and Gamelin, D. R. (2009). Dopant-carrier magnetic exchange coupling in colloidal inverted core/shell semiconductor nanocrystals. *Nano Lett.* 9, 4376–4382. doi: 10.1021/nl9026499

Wang, S. Z., Gao, R. M., Zhou, F. M., and Selke, M. (2004). Nanomaterials and singlet oxygen photosensitizers: potential applications in photodynamic therapy. *J. Mater. Chem.* 14, 487–493. doi: 10.1039/b311429e

Wu, Y., Zhen, Y., Ma, Y., Zheng, R., Wang, Z., and Fu, H. (2010). Exceptional intersystem crossing in di(perylene bisimide)s: a structural platform toward photosensitizers for singlet oxygen generation. *J. Phys. Chem. Lett.* 1, 2499–2502. doi: 10.1021/jz1008328

Xia, P., Raulerson, E. K., Coleman, D., Gerke, C. S., Mangolini, L., Tang, M. L., et al. (2020). Achieving spin-triplet exciton transfer between silicon and molecular acceptors for photon upconversion. *Nat. Chem.* 12, 137–144. doi: 10.1038/s41557-019-0385-8

Xiao, L., Gu, L., Howell, S. B., and Sailor, M. J. (2011). Porous silicon nanoparticle photosensitizers for singlet oxygen and their phototoxicity against cancer cells. *ACS Nano* 5, 3651–3659. doi: 10.1021/nn1035262

Yang, B., Chen, Y., and Shi, J. (2019). Reactive oxygen species (ROS)-based nanomedicine. *Chem. Rev.* 119, 4881–4985. doi: 10.1021/acs.chemrev.8b00626

Yogo, T., Urano, Y., Ishitsuka, Y., Maniwa, F., and Nagano, T. (2005). Highly efficient and photostable photosensitizer based on BODIPY chromophore. *J. Am. Chem. Soc.* 127, 12162–12163. doi: 10.1021/ja05 28533

You, Y. (2018). Chemical tools for the generation and detection of singlet oxygen. *Org. Biomol. Chem.* 16, 4044–4060. doi: 10.1039/C8OB 00504D

You, Y., and Nam, W. (2014). Designing photoluminescent molecular probes for singlet oxygen, hydroxyl radical, and iron-oxygen species. *Chem. Sci.* 5, 4123–4135. doi: 10.1039/C4SC01637H

Zheng, X., Wang, L., Liu, M., Lei, P., Liu, F., and Xie, Z. (2018). Nanoscale mixed-component metal–organic frameworks with photosensitizer spatial-arrangement-dependent photochemistry for multimodal-imaging-guided photothermal therapy. *Chem. Mater.* 30, 6867–6876. doi: 10.1021/acs.chemmater.8b 03043

Zhi, B., Mishra, S., Hudson-Smith, N. V., Kortshagen, U. R., and Haynes, C. L. (2018). Toxicity evaluation of boron- and phosphorus-doped silicon nanocrystals toward *Shewanella oneidensis* MR-1. *ACS Appl. Nano Mater.* 1, 4884–4893. doi: 10.1021/acsanm.8b01053